# A Heuristic Model of the Seasonal Cycle in Energy Fluxes and Climate

Aaron Donohoe* and David S Battisti*

*Department of Atmospheric Sciences, University of Washington, Seattle, Washington

(Manuscript submitted 03 September 2009)

*Corresponding author address:* Aaron Donohoe, University of Washington, 408 ATG building, box 351640, Seattle, WA, 98195
Email: aaron@atmos.washington.edu

**ABSTRACT**

In the annual mean, the polar regions receive a deficit of solar insolation relative to the global average. The local energy budget is balanced primarily by atmospheric heat transport into the region, with smaller contributions from ocean heat transport and anomalously low outgoing longwave radiation (relative to the global average). In contrast, the annual cycle features large seasonal anomalies (departures from the local annual average) in solar insolation in the polar regions that are primarily balanced by ocean heat storage anomalies; changes in meridional heat transport, emitted long wave radiation, and atmospheric heat storage play a decreasingly important role in the seasonal energy balance. Land-ocean contrasts also have a large impact on the seasonal energetics of the polar climate system. Over the ocean, zonal heat transport from the land domain is maximized during the summer, and the sum of the insolation and zonal heat transport anomalies is balanced by ocean heat storage. In contrast, over the land, the primary summertime balance is excess solar insolation balanced by an enhanced zonal heat export.

In this study we examine the global scale climate and the aforementioned seasonal cycle of energy fluxes using an aquaplanet atmospheric general circulation model coupled to a slab ocean and a simplified energy balance model that interacts with the underlying ocean. The gross climate and seasonal energetics in both models are highly sensitive to the specification of ocean mixed layer depth.

The observed seasonal cycle of energy fluxes and the land and ocean temperatures are also replicated in a simplified energy balance model that includes land-ocean contrast and the hemispheric differences in fractional land area. The sensitivity of the seasonal

cycle in climate (atmosphere and ocean temperatures) – and in the gross partitioning of the mix of energy flux processes that determine the climate – to the fractional land area is further explored in an ensemble of energy balance model integrations. In both the aquaplanet and land-ocean contrast energy balance models, the partitioning of energy fluxes amongst different physical processes can be understood in terms of the sensitivity of those processes to temperature perturbations. These experiments collectively demonstrate the effect of ocean mixed layer depth and fractional land area on climate and the seasonal partitioning of the various energy flux processes.

## 1. Introduction

A fundamental property of the Earth's climate system is the equator to pole gradient in solar insolation entering the atmosphere, leading to a gradient in absorbed solar radiation (ASR). While some of the gradient in solar radiative heating is ameliorated by the equator to pole gradient in the outgoing longwave radiation (OLR), the latter gradient is substantially weaker than the former (Fig. 1a) leading to regions of net radiative gain in the tropics and loss in the polar regions. Ultimately, almost all atmospheric and oceanic motions derive their energy from gradients in net radiation. In the annual mean there can be no net energy storage in a stable climate system and the top of atmosphere net radiative surplus (deficit) over the tropics (polar regions) most be exactly balanced by energy export (import) by way of atmospheric and oceanic motions. From the perspective of the atmosphere, the annual mean oceanic heat transport divergence manifests itself as an annual mean surface heat flux (SHF) and plays a substantially smaller role in the high latitude energy balance than does the atmospheric heat flux divergence.

The dominant spatial pattern in the top of atmosphere radiation – and hence in the atmospheric and oceanic heat flux divergence – is an equator to pole gradient. Hence, it is convenient to spatially integrate each quantity over equal area domains equatorward and poleward of $30^0$ which we will define as the tropics and the polar regions, and subtract the global annual average. In the annual average (Table 1, first row), for example, the Northern Hemisphere (NH) polar region receives a 7.9 PW deficit of ASR, relative to the global average. This deficit is partially offset by an OLR deficit of 2.2 PW that acts as an effective energy gain. The regional energy balance therefore requires an atmospheric and

oceanic heat transport divergence of 5.7 PW; this is equivalent to the total heat transport across $30^0$N by Gauss's Theorem: 4.3 PW coming from atmospheric meridional heat transport (MHT) and the remaining 1.4 PW entering the atmosphere by way of an annual mean SHF resulting from meridional ocean heat transport.

On seasonal time scales, the polar regions experience modulations in incoming solar radiation that are comparable in magnitude to the annual average insolation received in those regions; high latitude regions receive little or no solar insolation during the winter and upwards of 500 W/m$^2$ of daily mean insolation during the summer (150% of the globally averaged value and the maximum daily mean insolation value of anywhere on the planet). In contrast to the annual mean energy balance, the climate system does not achieve a balance between net radiation and meridional heat transport on seasonal time scales: energy is stored in either the surface (land or ocean) or the atmospheric column. For example, during the summer when the high latitudes absorb more solar insolation (than their annual mean value), a pseudo energy balance[1] can be achieved by: (i) increasing OLR and thus reducing the net radiation, (ii) reducing the atmospheric meridional heat transport, (iii) storing energy in the atmospheric column, thereby inducing a column averaged temperature tendency (CTEN), or (iv) storing energy beneath the surface/atmosphere interface (i.e. in the ground or ocean) by way of a SHF anomaly. The climatological and zonal averaged structures of these terms are shown for January and July in Fig. 1c, after removal of the zonal and annual averaged value from

[1] We use the term pseudo energy balance to refer to the fact that the system is not in equilibrium and is gaining or losing energy on seasonal time scales. We therefore define a closed system with respect to the atmosphere by including a term that accounts for negative the vertically integrated atmospheric energy tendency, or the energy that is stored locally.

each term. We note that the seasonal imbalances are of comparable magnitude to the annually averaged balance and that the predominant high latitude balance is achieved between excess ASR being balanced by changes in SHF with adjustments in OLR and MHT playing a secondary role and CTEN anomalies being approximately an order of magnitude smaller. In the framework of our polar and tropical regions, the polar seasonal ASR anomalies are of order 15PW, and are balanced by compensating anomalies in SHF, OLR, MHT and CTEN in an approximate ratio of 9:3:2:1. Understanding the relative magnitudes and controls of the seasonal energy partitioning amongst these processes on a global scale is the basis of this paper.

In addition to the large anomalies in the zonally averaged seasonal energy fluxes, there are equally large seasonal departures in the zonal anomaly energy balances over the land and ocean at a common latitude (Fig 1c and 1d). Because the heat capacity of the ocean mixed layer (the layer that changes temperature seasonally) is much greater than that of the land surface layer, the majority of the seasonal energy storage and therefore the seasonal anomalies in SHF occur over the ocean. Consequently, the seasonal cycle of atmospheric temperature over the ocean is strongly buffered, leading to a warmer atmosphere over the ocean as compared to the atmosphere over land at the same latitude during the winter and vice versa during the summer. Furthermore, because the atmosphere is remarkably efficient at transporting mass and heat zonally, there is a large seasonal cycle in the zonal energy flux down the land-ocean temperature gradient. For example, during the winter, the atmosphere overlaying the polar ocean receives 8 PW more SHF from the ocean than the atmosphere overlaying the polar land mass receives

from the land; this excess surface heat flux over the ocean is balanced a nearly equivalent quantity of zonal energy export to the land (Table 1).

The annually averaged energy balance has been studied extensively and both the fundamental constraints on the system and the balance achieved by the Earth are well documented in the literature. Stone (1978) realized that, because the meridional structure of solar-insolation and the outgoing longwave radiation (dictated by the local temperature) is dominated by the equator to pole gradient, the heat transport must be smooth and peaked in the mid-latitudes in order to achieve a balance with the net radiation. However, given a specified equator to pole gradient in solar insolation, these *a priori* constraints say very little about the relative magnitude of total heat transport and outgoing longwave radiation gradients (Enderton and Marshall 2009 ); in the context of the polar domain defined in this paper, while the 7.9 PW deficit in ASR must equal the sum of total heat transport and the polar OLR deficit, the relative partitioning of the latter two is unknown *a priori* and determined by their relative sensitivities to temperature gradients. Trenberth and Caron (2001) and Wunsch (2005) have documented the balance in the Earth's climate system and find that approximately 5.5 PW of heat is transported across $35^0$, in fair agreement with our values from Table 1 over a slightly different domain. This suggests that the meridional heat transport is more sensitive to temperature gradients than outgoing longwave radiation; we will re-examine this point in the body of the text.

On seasonal time scales, less theoretical and observational work has appeared in the literature. Fasullo and Trenberth have documented the seasonal cycle of the global mean energy balance (2008a), the meridional structure of the energy fluxes (2008b)

including the associated observational errors and seasonal balances over the land and ocean separately. We take these calculations as a foundation for the present work and attempt to understand, in a highly simplified framework, what dynamical and radiative processes control the seasonal cycle of the radiative and dynamical energy fluxes between the various components of the climate system. Furthermore, we ask which of the dominant seasonal energy balances are dictated by the physics of the system versus the specific geometry of the Earth's climate system. Our tool of choice for these tasks is a seasonal energy balance model (EBM), linearized about a global annual mean basic state.

EBMs have been used extensively to study the annual mean climate system (i.e. Budyko 1969, Sellers 1969, and North 1975) and the seasonal climate (i.e. Sellers 1973, North and Coakley 1978, and Thompson and Schneider 1979). These models are useful because they reduce the climate system to a minimal number of control parameters and diagnostic variables, thus making the model behavior (in our case, the flow of energy) easily tractable. Our seasonal EBM adopts similar elements to those previously documented but has a simplified meridional structure, allowing us to isolate the equator-to-pole scale seasonal energy processes and illuminate the sensitivity of those processes to model parameters. Our focus is more on the seasonal, global scale flow of energy in the system, as discussed in this section, and less on the intricate meridional structures.

The outline of the paper is as follows. We describe the EBM and additional data used in this work in Section 2. In Section 3, we document aquaplanet simulations with our energy balance model and compare the seasonal energy flow to slab ocean aquaplanet atmospheric general circulation model (AGCM) simulations with different ocean depths. In Section 4, we explore the implications for climate of the seasonal cycle of energy flow

between the land and ocean domains and the sensitivity of the climate to the specified fractional land cover. A summary and discussion follows.

## 2. Models and data sets used in this study

We describe in section (a) below the zonally symmetric aquaplanet seasonal EBM used in this study as well the seasonal EBM that includes a simple representation of land-ocean contrasts (further details are provided in the Appendix). We then briefly describe an aquaplanet AGCM that is coupled to a slab ocean to complement the results from the aquaplanet EBM in section (b). The data sets used in this study are listed in section (c).

### *a. Seasonal energy balance models*

The physics and numerics of the EBMs are briefly documented in this subsection. The parameterizations chosen are based on linear regressions between the EBM variables (surface and atmospheric temperatures) and the energy fluxes in the observational record or, in some cases, in GCM simulations; a more detailed description of all the parameterizations is provided in the Appendix.

#### 1) SINGLE COLUMN BASIC STATE

The zonally symmetric (aquaplanet) and zonally asymmetric (incorporating land-ocean contrasts) EBMs are cast as (linear) anomaly models about a basic resting state atmosphere that is in radiative-convective equilibrium with the annual, global mean absorbed solar radiation (239 $Wm^{-2}$). In the vertical, the energy balance model consists of three atmospheric levels and a single surface layer. The emissivity ($\varepsilon$) of each atmospheric layer is determined by the local temperature, an assumed fixed relative

humidity of 75% and, $CO_2$ concentration of 350 ppm according to Emanuel's (2002) parameterization. The basic state is calculated assuming the following: (i) the prescribed absorbed solar radiation is absorbed entirely at the surface; (ii) the surface layer behaves as a black body, absorbing all of the incident longwave radiation from the atmospheric layers and emitting radiation according to the surface temperature's Planck function; (iii) each atmospheric layer absorbs and emits longwave radiation according to its emissivity (and equivalent absorbtivity).

The latent heat flux (LHF) between the surface and the atmosphere is parameterized as

$$LHF = B_{LH} (T_S - C_{LH}), \quad (1)$$

where $T_s$ is the surface layer temperature $B_{LH}$ is 4 $Wm^{-2}K^{-1}$ and $C_{LH}$ is 270K (see Appendix for details on the values of these and other parameterizations and coefficients). This flux is removed from the surface layer and distributed in a 9:9:2 ratio amongst the lowest, middle, and highest atmospheric layers, roughly mimicking tropical observations (Yang et al. 2006). Similarly, the sensible heat flux (SENS) is parameterized as

$$SENS = B_{SH}(T_S - T_{A1} - C_{SH}), \quad (2)$$

where $T_{A1}$ is the lowest atmospheric layer temperature, $B_{SH}$ is 3 $Wm^{-2}K^{-1}$ and $C_{SH}$ is assessed to be 6 K from the data using 900 hPa as the reference level for the lowest atmospheric layer (Appendix A) but is adjusted to 24 K in the model (because our lowest level is higher in the atmospheric column). The sensible heat flux operates between the surface layer and lowest atmospheric layer only.

The single column atmosphere produces a basic state that is in radiative-convective equilibrium with the annual, global mean absorbed solar radiation (239 $Wm^{-2}$) that has the following temperature structure:

$$\overline{T_S} = 287K, \quad \overline{T_{A1}} = 262K, \quad \overline{T_{A2}} = 248K, \quad \overline{T_{A3}} = 225K\,. \tag{3}$$

The corresponding surface energy balance is +239$Wm^{-2}$ ASR, -170 $Wm^{-2}$ net longwave radiation, –69$Wm^{-2}$ latent heat flux, and negligible sensible heat flux with the signs defined relative to the surface layer. The lower, middle, and highest atmospheric layers have emissivities of .66, .38, and .29 respectively. This system represents a simplified global annual mean radiative convective balance. Next, we linearize the EBM about this basic state to form the seasonal zonally symmetric (aquaplanet) and asymmetric (land-ocean contrast) EBMs.

## 2) LINEARIZED THREE-BOX (AQUAPLANET) ENERGY BALANCE MODEL

We now build a model consisting of three meridional boxes representing the tropical and polar regions on a spherical planet with boundaries at $30^0$N and $30^0$S. Each meridional box has three atmospheric layers and a surface layer, linearized about the global annual mean basic state described in the previous section. The layer emissivities are fixed at their basic state values. The anomalous longwave radiation (LW') emitted by each layer takes the form of

$$LW_N^{'} = C_{WV}\varepsilon_N 4\sigma\overline{T_N}^3 T_N^{'} \equiv C_{WV}\varepsilon_N B_{OLR,N} T_N^{'}\,, \tag{4}$$

where $\sigma$ is Planck's constant $\varepsilon_N$ is the layer's emissivity (unity for the surface), $B_{OLR,N}$ is the local change in emitted longwave radiation per unit change of temperature (units of

$Wm^{-2}K^{-1}$) expected from the Planck function and $C_{WV}$ is a water vapor feedback factor (0.65 in the atmospheric layers and 1.0 at the surface) intended to capture the water vapor feedback as discussed in the Appendix. If an entire region were to warm uniformly in the vertical, the change of OLR with temperature is 2.6 $Wm^{-2}K^{-1}$, a value we will denote by $[B_{OLR}]$ (brackets represent a vertical average); approximately 30% of the radiation escaping to space originates from the surface layer. This value is analogous to our model's inverse climate sensitivity and is slightly higher than other values published in the literature (see Warren and Schneider 1979 for a review).

The linearized SENS and LHF fluxes do not depend on $C_{LH}$ and $C_{SH}$[2], so all of the surface energy flux anomalies are given by the surface temperature perturbations times the parameters $B_{LH}$ and $B_{SH}$; these can be readily by compared to the $B_{OLR,S}$ of 5.3$Wm^{-2}K^{-1}$ to assess the relative magnitudes of surface radiative, latent heat flux and sensible heat flux anomalies.

The heat transport between the tropical and polar boxes is by horizontal diffusion between the atmospheric layers in adjacent boxes. The vertically averaged atmospheric energy transport divergence reduces to the expression

$$MHT_{N,S} = B_{MHT}\left(\left[T_T'\right]-\left[T_{N,S}'\right]\right) , \qquad (5)$$

where the subscripts refer to the northern (N) and southern (S) polar and tropical (T) regions respectively, the brackets denote a vertical average, and $B_{MHT}$ is the diffusive coefficient, equal to 3.4 $Wm^{-2}K^{-1}$ corresponding to a diffusion value (D) of 0.95$a^2$ $Wm^{-2}K^{-1}$ ( a is the Earth's radius) as described the Appendix.

[2] The values of $C_{LH}$ and $C_{SH}$ have no direct effect on the linearized EBM since these terms only show up in the mean state equations and are therefore removed from the linearized system.

The ocean mixed layer depth is pre-specified in each set of experiments (we will explore the model sensitivity to this parameter in section 3b) and each atmospheric layer has an equal mass and therefore heat capacity. The model is initialized at the boreal autumnal equinox and run forward with time varying solar insolation for several years until it converges to steady seasonal cycle. We compute the amplitude of the seasonal cycle as the amplitude of the annual harmonic.

### 3) LINEARIZED, SIX-BOX ENERGY BALANCE MODEL THAT INCLUDES LAND-OCEAN CONTRAST

We take the 3-box model described in the previous section and divide each meridional box into ocean and land subdomains, with specified land fractions. The linearized column energetics are unchanged from before except that the latent heat flux over land is set to zero. The MHT is assumed to be zonally invariant and is determined from atmospheric temperatures, zonally averaged over the land and ocean subdomains.

The atmospheres over the land and ocean subdomains at the same latitude communicate by way of a zonal heat flux divergence:

$$ZHT_{O,L} = \frac{B_{ZHT}\left(\left[T_{L,O}\right]-\left[T_{O,L}\right]\right)}{F_{O,L}} \ , \qquad (6)$$

where the subscripts refer to the ocean (O) and land (L) subdomains at the given meridian, $B_{ZHT}$ has a value of 10 $Wm^{-2}K^{-1}$ (see appendix A.e), and $F_{O,L}$ is the ocean or land fraction in each meridional domain. By definition, the zonal heat flux between the ocean and land and vice versa, must be equal an opposite. However, the zonal heat flux divergence, which is more relevant for the local energetics, scales inversely as the

fractional area of surface type. The land surface layer is given a heat capacity of one third of the atmospheric column and we fix the ocean mixed layer depth at 60 meters in this series of experiments. The control six-box run specifies land fractions ($F_L$) of 10%, 25%, and 50% in the southern polar, tropical, and northern polar regions respectively, mimicking the Earth. Experiments in section 4d explore the response of the model to land fraction in an ensemble of runs with polar $F_L$ varying symmetrically in both hemispheres. All six-box runs are forced with seasonally varying ASR derived from a Fourier expansion of ERBE data (described in Section 2c), averaged over the respective meridional domains and truncated at the semi-annual component (inclusive). Table 2 summarizes the coefficients used in the energy balance model.

*b. Aquaplanet atmospheric general circulation model (AGCM) simulations*

We utilize an ensemble of aquaplanet AGCM simulations coupled to a slab ocean for comparison to our EBM predictions in Section 3. The ensemble members have prescribed slab ocean depths of 2.4, 6, 12, 24, and 50 meters. The model integrations are preformed with the Geophysical Fluid Dynamics Lab Atmospheric Model version 2.1 (Delworth et al. 2006) featuring a finite volume dynamical core (Lin 2004) with M45 L24 resolution. Each model is forced by seasonally varying solar insolation with zero eccentricity and $23.439^0$ obliquity, and is run for ten years which is sufficient to converge on a steady climatology. The model climatology is taken from the last five years of the integrations. The heat transport divergence is calculated as the residual of the sum of the net radiation, surface energy flux (SHF), and (minus) the storage term CTEN.

*c. Observational data*

The radiation data used in the introduction and for comparison in Section 4 is from ERBE satellite data (Barkstrom and Hall 1982) and has been adjusted for discontinuities in the observational system and diurnal aliasing (Fasullo and Trenberth, 2008a). The atmospheric heat transport and integrated column energetics are taken from updated calculations (http://www.cgd.ucar.edu/cas/catalog/) preformed by the National Center for Atmospheric Research according to methodology of Trenberth et al. (2001); we utilize fields that are derived from the National Center for Environmental Prediction reanalysis data to compute the observed seasonal energetics. The surface heat flux climatology is determined from the residual of the column energy tendency, top of the atmosphere net radiation, and heat flux convergence. All quantities discussed in the subsequent sections and figures are spatially averaged equatorward and poleward of $30^0$.

**3. Aquaplanet simulations from the energy balance model and AGCM**

In the introduction, it was shown that seasonal cycle in energy fluxes to the polar atmosphere is dominated by large amplitude oscillations in ASR, compensating oscillations in SHF of comparable magnitude, and changes in MHT, OLR, and CTEN playing a decreasingly important role in the regional seasonal energetics. We now attempt to answer the following questions:

(i) Why is the predominant seasonal balance in the observed climate system between ASR and SHF?

(ii) Can we imagine a climate system where the seasonal cycle of ASR is mostly balanced by another term (for example, OLR or MHT)?

(iii) What parameters control the partitioning of energy fluxes?

(iv) What controls the seasonal cycle of atmospheric and surface temperatures?

We force the linearized EBM with seasonally varying absorbed shortwave radiation (details in section 4b) and examine the seasonal cycle of energy fluxes. We begin our analysis with a brief discussion of the annual mean energy balance. We then present the temperature and energetics climatology as a function of ocean mixed layer depth in our aquaplanet EBM and the aquaplanet AGCM simulations.

*a. Annually averaged energy balance*

In the annual mean, there can be no heat storage in either the surface layer or atmospheric column in an equilibrated climate system. Therefore, in our EBM, the prescribed global anomaly ASR in the polar region of -7.9 PW must by balanced by meridional heat import and the negative of OLR anomalies (OLR is an energy loss). The EBM steady state solution is independent of the layer's heat capacity and consists of 5.5 PW of meridional heat import and 2.4 PW of energy gain by anomalously low OLR. These values compare reasonably well with the observations (Table 1) although the latter is complicated by both land-ocean contrast and ocean heat transport.

What determines the ratio of MHT to OLR anomalies in maintaining the polar annual mean energy balance? If we assume that all four vertical layers in both North and South polar regions have the same global temperature anomaly, $\Delta T$, global mean energy balance then requires that the tropical layers have an equal and opposite temperature anomaly (so global mean OLR is unchanged). If the annual mean system has minimal vertical structure, the MHT acts across a temperature difference of $2\Delta T$ where as the OLR anomaly is proportional to $\Delta T$. This, coupled with the relative sensitivities of the respective MHT and OLR energy fluxes to temperature anomalies, suggest that

$$\frac{\overline{MHT}}{\overline{OLR}} \approx \frac{2B_{MHT}}{[B_{OLR}]} = \frac{7.5(\frac{D}{a^2})}{[B_{OLR}]} = 2.6\,, \tag{7}$$

where $D$ is the temperature diffusivity of the system[3]. The ratio 2.6 is close to the actual value from the EBM of 2.3: the difference is due to the vertical structure in the true steady state solution which has larger temperature anomalies at the surface than those aloft ($\Delta T$ is 8.6K for the surface and 6.4K averaged over the atmosphere). This ratio plays a critical role in determining whether the system reaches a diffusive or a radiative equilibrium; in the limits of $D$ approaching zero and infinity, the annual mean heat transport into the polar region is 0 and 7.9 PW, respectively.

*b. Seasonal temperatures and energy fluxes*

It is widely recognized that the thermal inertia of the ocean plays a critical role in buffering the seasonal cycle of atmospheric and surface temperature (e.g., Hartmann 1994). We explore the role of ocean heat storage on seasonal energetics in an ensemble of aquaplanet EBM and AGCM simulations with varying ocean mixed layer depths. The seasonal cycle of solar insolation in the GCM runs has no precessional cycle. The seasonal ASR anomalies used to force the EBM are prescribed from a Fourier expansion of the 12 meter depth GCM seasonal ASR anomalies, averaged over each meridional domain, truncated at the semi-annual component (inclusive).

The amplitude of the seasonal cycle in surface and atmospheric temperatures decreases (roughly inversely) with mixed layer depth in the EBM; results from the aquaplanet GCM agree remarkably well with those from the EBM (Fig. 2a).

[3] The conversion between D and $B_{MHT}$ is discussed in Appendix 1.d.

The amplitude and relative importance of the various energy flux terms that balance the ASR in the polar region are also a strong function of the mixed layer depth (Fig. 2b). For deeper mixed layer depths, the seasonal cycle in ASR in the polar region (amplitude 18.6 PW) is primarily balanced by SHF while, at shallower mixed layer depths, the seasonal cycle of MHT, OLR, and CTEN play a more prominent role in maintaining the seasonal pseudo energy balance. The seasonal amplitude of each energy flux term as a function mixed layer depth in the aqua planet GCM is qualitatively captured by the EBM simulations, as is the relative magnitude of one term compared to another term.

Understanding the qualitative behavior of the seasonal energy fluxes as the ocean deepens in the EBM is straightforward. All ASR anomalies go directly into the surface layer, and are only communicated to the atmospheric layers via latent, sensible, and radiative energy flux anomalies. Therefore, ASR anomalies only make their way to the atmosphere by heating the surface layer and consequentially changing the upward energy flux. As the ocean mixed layer deepens, more of the solar energy goes into heating the surface layer, appearing as a SHF anomaly to the atmosphere, and less of the solar energy enters the atmosphere, because the seasonal surface temperature anomaly is reduced.

The partitioning of the net energy entering the atmosphere into MHT, OLR, and CTEN is also readably understandable within our model framework. Ultimately, all atmospheric energy fluxes result from temperature anomalies within the atmosphere, with the magnitude of the various energy fluxes dictated by the B coefficients for the respective processes. The column tendency pseudo-energy flux complicates this framework because it is governed by temperature tendencies as opposed to temperature

anomalies. We can compose an effective $B_{CTEN}$ by assuming that the seasonal temperature cycle is composed entirely of the annual Fourier component. The derivative of the temperature scales as the amplitude of the temperature anomalies times the radial frequency of the annual cycle, resulting in

$$B_{CTEN} = \frac{2\pi[Cp]}{1\ year} = 2.0\ Wm^{-2}K^{-1} \quad , \tag{8}$$

where $Cp$ is the atmospheric heat capacity. The pseudo energy flux associated with CTEN will temporally lag the MHT and OLR signals, but only by a small phase as discussed later in this section. The relative amplitudes of the seasonal MHT:OLR:CTEN is then given by

$$MHT : OLR : CTEN = B_{MHT} : [B_{OLR}] : B_{CTEN} \quad , \tag{9}$$

or approximately 7:5:4 in our model[4]. This relationship is remarkably consistent for all mixed layer depth EBM simulations. Furthermore, the aquaplanet AGCM ensemble also has a consistent MHT:OLR:CTEN seasonal amplitude ratio of approximately 14:11:10 in all the ensemble runs , suggesting that these linear ideas may be applicable to more complicated model integrations. The precise ratios of energy flux amplitudes differ between the EBM and aquaplanet AGCM. Most notably, the CTEN and OLR amplitudes are nearly equal in the AGCM, suggesting that the AGCM's $[B_{OLR}]$ is closer to 2 $Wm^{-2}K^{-1}$ (since $B_{CTEN}$ is essentially fixed by the atmospheric mass).

In the EBM, the ratio of the seasonal amplitude of the polar surface temperature to the atmospheric temperature is remarkably constant at 1.01; the same ratio in the

[4] Note that we use $B_{MHT}$ instead of $2B_{MHT}$ (as was used for the annual mean) because the tropical temperatures have a minimal seasonal cycle.

aquaplanet AGCM has an average of 1.06 and varies slightly amongst the ensemble members (standard deviation of .06). We can understand these results in the model framework by first noting that the atmospheric temperatures are very nearly in pseudo-equilibrium with the energy input from the surface; in the absence of other energy inputs, atmospheric temperatures would approach equilibrium with an e-folding time scale of

$$\tau_{atmos} = \frac{[Cp]}{[B_{LW\uparrow}] + [B_{LW\downarrow}] + B_{MHT} + B_{SH}} = 11 \ days \ , \qquad (10)$$

where $[B_{LW\uparrow}]$ and $[B_{LW\downarrow}]$ are the change in upwelling and downwelling longwave radiation leaving the atmosphere per unit change in the atmospheric column and have values of 1.9 and 2.2 $Wm^{-2}K^{-1}$ respectively (Table 2). Since the atmosphere is in pseudo-equilibrium on seasonal time scales, the input of energy into the atmosphere by way of the sensible heat, latent heat, and surface radiative fluxes must equal the export of energy from the polar atmosphere via longwave radiation, CTEN, and MHT. Assuming the seasonal tropical temperature changes are small, each of these quantities can be expressed in terms of either the surface or atmospheric temperature anomaly resulting in the expression

$$\frac{\left|T_S^{'}\right|}{\left|[T_A^{'}]\right|} = \kappa = \frac{B_{SHF} + B_{MHT} + [B_{LW\uparrow}] + [B_{LW\downarrow}] + B_{CTEN}}{B_{SHF} + B_{LHF} + B_{OLR,S}} = 1.0 \, . \qquad (11)$$

We can understand the physical basis of equation (11) by taking the not so hypothetical example of reducing the efficiency of surface heat export (the denominator of Equation 10) by, say, reducing the LHF feedback as would happen over a land surface. In this case, as the insolation heats up the surface, less energy is fluxed from the surface to the atmosphere (than with the LHF feedback turned on). Consequently, more of the energy from ASR is retained in the surface and the seasonal amplitude of the surface temperature

will increase; the component of the coupled system (surface and atmosphere) that is least efficient at exporting energy will experience the largest temperature anomalies. The above argument is supported by experiments whereby the EBM parameters are tweaked and the κ values predicted by (11) are verified by the EBM integrations (not shown). The parameters of our aquaplanet EBM suggest that the atmosphere and ocean surface are nearly equally efficient at exporting heat, resulting in equal amplitudes of the temperature seasonal cycles. The aquaplanet AGCM simulations also have atmosphere and surface temperature seasonal cycles that are nearly equivalent in magnitude. We will revisit this analysis using a more realistic system that includes zonal land-ocean contrast in Section 4 and find that atmosphere is substantially more efficient than the surface at exporting heat in the presence of zonal asymmetries in surface heat capacity.

We now attempt to understand the percentage of seasonal ASR anomalies that is stored in the ocean ($E_{OC}$) as opposed to the energy that is eventually fluxed to the atmosphere ($E_{ATMOS}$) to drive seasonal changes in MHT, OLR and CTEN. To begin, we calculate the amplitude of the energy tendency within the ocean mixed layer per unit of temperature change, approximating the temperature anomalies as the annual harmonic:

$$B_{OC} = \frac{2\pi \, \mathrm{C}_{H_2O} \, \rho_{H_2O} \, H}{1 \ year}. \tag{12}$$

As the ocean warms seasonally, it fluxes more energy to the atmosphere above and the atmosphere comes into equilibrium fairly rapidly, balancing the enhanced energy input radiatively, dynamically, and through storage. The ocean heat uptake and surface heat flux to the atmosphere is in phase quadrature, because the ocean cannot flux additional heat to the atmosphere until it heats up. In contrast, the seasonal cycle in the atmospheric terms CTEN, MHT, and OLR are nearly in phase with each other. The ratio of $E_{OC}$ to

$E_{ATMOS}$, assuming the atmosphere comes into pseudo-equilibrium with a temperature change of κ times the ocean temperature change, is

$$\frac{E_{OC}}{E_{ATMOS}} = \frac{|SHF'|}{|MHT'|+|OLR'|+|CTEN'|} = \frac{B_{OC}}{B_{SH}(1-\kappa^{-1})+B_{LH}+B_{OLR,S}-\kappa^{-1}[B_{LW\downarrow}]}. \quad (13)$$

This ratio -- coupled with the constraints that the seasonal amplitude of $E_{OC}$ and $E_{OLR}$ must add (in quadrature) to the prescribed seasonal amplitude of ASR and that the ratio of MHT, OLR, and CTEN is fixed (as discussed previously) -- allows the amplitudes of SHF, MHT, OLR, and CTEN to be determined uniquely as a function of ocean mixed layer depth and the other model parameters. The amplitude of each of the seasonal energy flux terms using the pseudo steady state approximations (Equations 8-13) are shown in Figure 2 (dashed lines), and are comparable to those from the EBM (solid lines) and the aquaplanet GCM simulations. The agreement between the pseudo-equilibrium predictions and the EBM output is not exact because the modeled atmosphere is not completely in steady state, especially for the simulations with a shallow ocean mixed layer. Nonetheless, the general agreement suggest that the ideas presented above are applicable to the EBM and that we can approximately solve for the systems behavior, given the model control parameters, without performing numerical integrations.

**4. Land-ocean simulations with the six-box energy balance model**

In the observations, zonal asymmetries in seasonal energetics that result from land-ocean contrasts are comparable in magnitude to the zonal mean seasonal energetics. Here, we explore these processes in our six-box EBM model framework. We start by looking at a control run, intended to simulate the land configuration in each hemisphere

in the real world and forced by the observed seasonal cycle of ASR. In addition to analyzing the seasonal energetics over the land and ocean domains, we also ask how the different land fractions in the NH and Southern Hemisphere (SH) affect the globally averaged and zonal mean seasonal energetics. We then explore the impact of land and ocean fraction on the seasonal energy balance in an ensemble of EBM runs.

*a. Globally averaged energetics*

The planet currently receives more solar insolation during the boreal winter, when it is closest to the sun, corresponding to approximately 6 PW of additional insolation arriving at the top of the atmosphere (Berger 1978). The seasonal cycle of global averaged ASR is in phase with the incoming insolation but substantially smaller in magnitude (of order 3PW) due to seasonal changes in the planets effective albedo[5] (Fasullo and Trenberth 2008a). Global mean OLR is in phase with Northern Hemisphere insolation (Fig. 3) and is therefore out of phase with the ASR, resulting in a net radiation into the climate system during boreal winter that exceeds the global ASR seasonal amplitude in magnitude. This radiative imbalance is primarily balanced by ocean heat uptake (SHF), with CTEN playing a smaller role.

Our land-ocean EBM qualitatively reproduces the phasing of the various components of the global mean seasonal energetics. In the NH, the enhanced land fraction causes a larger seasonal magnitude of surface temperature and greater seasonal heat flux to the atmosphere leading to larger seasonal magnitudes in OLR and CTEN than

[5] The seasonal cycle of effective, or insolation-area weighted, albedo is dominated by a semi-annual oscillation associated with the solar insolation shifting from the tropics to the polar regions where the albedo is larger. In situ surface property changes make smaller contributions to effective albedo.

those in the Southern Hemisphere (SH), where most of the ASR enters the ocean mixed layer. Thus, the global mean OLR and CTEN phasing is essentially dictated by the hemispheric differences in land fractions, independent of the precessional phasing. We can verify this behavior in the EBM by shifting the precession by six months: the phasings of OLR and CTEN are unchanged (not shown) and the dominant global mean energy balance features an increased ASR during the boreal summer that is balanced by an increased OLR, with seasonal ocean heat storage playing a much smaller role. This experiment suggests that global averaged seasonal energetics may have been very different in different paleoclimate states.

*b. Zonal mean energetics*

The observed and EBM control simulation of the seasonal energy fluxes averaged over the land and ocean sub-domains in each meridional box are shown in Fig. 4. The asymmetry between Hemispheres is primarily due to the hemispheric differences in polar land fraction and, in small part, to the precessional signal in the prescribed ASR. Most notably, the EBM seasonal amplitude of SH SHF is 14.5 PW as compared to 9.9 PW in the NH, which compares favorably to the observed amplitudes of 13.4 and 10.2 PW respectively. This result follows from the fact that the ocean surface layer must absorb a much larger quantity of energy than land before it achieves the same temperature anomaly as the land surface and subsequently fluxes a similar amount of energy to the atmosphere. Hence, a greater fraction of the seasonal ASR anomaly is fluxed to the atmosphere in the NH compared to the SH, producing greater amplitudes in the seasonal cycle of OLR, CTEN, and MHT in the NH compared to the SH. These results agree favorably with the observations.

Fig. 4 also illustrates the magnitude of errors induced by neglecting ocean heat transport in our EBM. By definition, the annual mean EBM SHF in each meridional domain is zero. The annual averaged SHF in nature is balanced by the vertically integrated ocean heat transport convergence. The ocean heat transport into the NH and SH polar boxes contribute to mean offsets between the observed and EBM simulated SHF seasonal cycles of +1.4 and +.9 PW respectively. These numbers are significant and certainly impact the annually averaged energetics. They are, however, an order of magnitude smaller than the seasonal SHF anomalies, suggesting that the ocean's influence on *zonally averaged* climate is primarily through its thermal inertia, and secondarily by way of its dynamical heat flux (Seager et al., 2002).

*c. Land-ocean energetics*

The seasonal cycle of energy fluxes from the EBM control run for the land and ocean subdomains are shown in Figure 5. Over the ocean in the NH, the SHF is of opposite sign and larger in magnitude than the ASR: during the summer, more energy gets put into ocean storage than is received from the sun, with the additional energy coming primarily from the zonal transport of heat (ZHT) away from the warmer land subdomain. In contrast, the predominance of ocean in the SH reduces the magnitude of ZHT in the ocean subdomain (because there is a larger area to distribute the heat fluxed from land to ocean) and the dominant seasonal balance is between ASR and SHF only, with limited seasonal cycles in MHT, OLR, and CTEN. The SH ocean sub-domain behaves similarly to the aqua-planet EBM simulation with a 60 meter mixed ocean depth.

Over the polar land sub-domains, there is very little seasonal storage in the surface layer. Therefore, the majority of the energy entering the system through ASR

finds its way into the atmosphere where it must be fluxed away (ZHT and MHT), radiated to space (OLR), or stored (CTEN). The seasonal magnitude of these terms, assuming they are all in phase, must add to the seasonal amplitude of ASR. The relative partitioning of energy across these terms is not as simple as the ratio of the B coefficients, however, because the ZHT relies on the land-ocean atmospheric temperature contrast and the temperatures above the ocean are also evolving seasonally. Furthermore, the MHT is determined by the zonal average atmospheric temperature in our formulation of the EBM. Hence, changes in meridional diffusion due to polar temperature changes in the land (ocean) sub-domain lead to smaller (larger) changes in MHT than would be expected based on the value of $B_{MHT}$ because the magnitude of atmospheric temperature changes in the ocean (land) sub-domain are smaller (larger). Nonetheless, we can recognize that an isolated, instantaneous atmospheric temperature perturbation in the polar land-subdomain will induce energy flux changes that are proportional to the respective B coefficients. $B_{ZHT}$ divided by land fraction has values of 20 and 100 $Wm^{-2}$ in the NH and SH respectively; ZHT is therefore responsible for 65% and 90% of the total instantaneous atmospheric energy flux adjustment in the respective hemispheres. It is therefore not surprising that the large ASR anomalies over land are primarily compensated for by ZHT, and more so in the SH than in the NH. ZHT is the fastest (most sensitive) process in the climate system and, thus, the amplitude of the seasonal cycle over land in the polar SH and throughout the polar NH domain hinges critically on the land-ocean temperature contrast.

*d. Land fraction experiments*

The previous subsection suggested that the fractional land area ($F_L$) in the NH and SH had a profound effect on the local energetics. We now explore this parameter space more completely in an ensemble of EBM integrations with varying polar land fractions (symmetric about the equator), forced by ERBE derived seasonal ASR anomalies. Fig. 6 summarizes the seasonal amplitudes of the temperatures and energetics over the polar sub-domains as a function of $F_L$.

1) DESCRIPTION OF RESULTS

The energy balance model shows that the amplitude of the surface temperature over land doubles from 15 to 30C as the land fraction increases from near zero to near one. Increasing the land fraction causes and even larger increase in the amplitude of the seasonal cycle of atmospheric temperatures over land and ocean: from about 3K at near zero land fraction to 16K with nearly all land. The amplitude of the seasonal cycle in ocean temperature spans from 3K with nearly all ocean to 5K with a very large land fraction. The qualitative aspects of the climate response is not surprising: increasing the land fraction causes the seasonal cycle of temperatures to increase because a greater fraction of the seasonal ASR anomalies are delivered straight to the atmosphere by surface heat fluxes – nearly in phase with the ASR -- and less is stored in the ocean (to be released to the atmosphere six months out-of-phase with the ASR).

The partitioning of the energy flux between the various processes as a function of land fraction over land and ocean is shown in Fig. 6b and 6c, respectively. The sensitivity in the seasonal cycle of climate as a function of land fraction (displayed in Fig 6a and discussed above) is largely due the zonal advection of energy. With no zonal advection, the amplitude of the seasonal cycle in atmospheric temperature over land would greatly

exceed that over ocean, and lead the latter by about three months. Zonal advection balances out the temperature differences, mainly moving the excess (deficit) insolation in summer (winter) to the atmosphere overlaying the ocean in a matter of days. As the land fraction becomes small, this export term becomes very large ($105 W/m^2$)– nearly canceling the seasonal excess in ASR ($120 W/m^2$). Of course, the exported energy over land is a source of energy for the atmosphere over the ocean, a portion of which is emitted downward to add (in phase) with the seasonal cycle in ASR – enhancing the seasonal cycle of surface temperature in the ocean: the greater the land fraction, the more energy is exported from land to ocean (in phase with the ASR).

Finally, the seasonal cycle in the amplitude of the MHT and OLR also increase with increasing land fraction, in the net and over ocean and land. This result follows simply because the seasonal cycle in the surface temperature over land increases with increasing land fraction. This increases the amplitude of the seasonal cycle of heat flux to the atmosphere (in phase with the surface temperature and ASR) and so too an increase in the amplitude of the atmospheric temperature over land (and by zonal advection, over ocean). Hence, increasing land fraction causes the seasonal cycle of both OLR and MHT to increase (the latter follows because the seasonal cycle of air temperature in the tropics is small). In the next section, we perform a scaling analysis to understand the qualitative and quantitative relationships between the fraction of land and the amplitude of the seasonal cycle in climate and the partitioning of energy fluxes between the various terms that are shown in Figure 6.

### 2) Analysis of results

Perhaps the most robust result is that, independent of the $F_L$, the seasonal amplitude of surface temperature exceeds that of atmospheric temperature in the land sub-domain, where as the opposite is true over the ocean. For example, with 50% land, the ratio of $T_S/T_A$ is about 2.7 in the land subdomain and 0.5 in the ocean subdomain. This result seems physically intuitive given the reduced thermal inertia of the land surface as compared to the ocean leading to large land surface temperature tendencies. There is a compensating process, however: the enhanced seasonal amplitude of surface temperature, *ceteris paribus*, will induce proportionally larger amplitude seasonal energy fluxes from the surface to the atmosphere. Nonetheless, we still expect that the seasonal amplitude of surface and atmospheric temperature to be governed by equation (11), modified to account for both the ZHT between the land and ocean subdomains and the lack of LHF over land:

$$\frac{\left|T'_{S,L}\right|}{\left|\left[T'_{A,L}\right]\right|} = \kappa_L = \frac{B_{SHF} + B_{MHT}(F_L + \Delta(1-F_L)) + \left[B_{LW\uparrow}\right] + \left[B_{LW\downarrow}\right] + B_{CTEN} + \frac{B_{ZHT}(1-\Delta)}{F_L}}{B_{SHF} + B_{OLR,S}}, \quad (14)$$

with $\Delta$ the ratio of atmospheric temperature anomaly over ocean to that over land:

$$\Delta = \frac{\left[T_{A,O}\right]}{\left[T_{A,L}\right]} \quad . \quad (15)$$

We can evaluate the effect of removing the LHF only, by setting $F_L$ and $\Delta$ to one in (14), in which case $\kappa_L$ becomes 1.5, substantially smaller than the typical ratio of approximately 3 realized in the EBM simulations (Fig. 6a). Clearly, the land-ocean coupling plays a critical role in setting $\kappa_L$ by moving excess energy fluxed to the atmosphere from the seasonally heated land surface to the ocean domain before the atmospheric column heats up. Though solving (14) requires knowledge of $\Delta$, $\Delta$ must be

less than one due to the greater fraction of ASR making its way into the atmosphere over land via the surface heat flux. Hence, ZHT greatly increases the seasonal amplitude of the surface temperature relative to atmospheric temperature ($\kappa_L$) in the land subdomain in (14).

Over ocean, the amplitude of the seasonal surface temperature to atmospheric temperature $K_O$ is again given by a modified version of equation (11):

$$\frac{\left|T'_{S,O}\right|}{\left|\left[T'_{A,O}\right]\right|} = \kappa_O = \frac{B_{SHF} + B_{MHT}\dfrac{F_L\Delta^{-1} + (1-F_L)}{2} + \left[B_{LW\uparrow}\right] + \left[B_{LW\downarrow}\right] + B_{CTEN} + \dfrac{B_{ZHT}(1-\Delta^{-1})}{F_L}}{B_{LHF} + B_{SHF} + B_{OLR,S}}. \qquad (16)$$

The ZHT decreases $K_O$ by adding energy to the atmosphere overlaying the ocean during the warm season. Essentially, because the atmospheric temperature anomalies have a greater magnitude over land ($\Delta<1$), the direction of ZHT is dictated by the atmospheric temperatures in the land subdomain, thus acting as a negative (positive) feedback to atmospheric temperatures in the land (ocean) domain.

We can make some progress in understanding the coupled system by noting that, in the limit of a small $F_L$, the ocean sub-domain behaves similarly to the 60 meter aquaplanet. In this case Equation (13) states that 85% of the seasonal energy from ASR is stored in the slab ocean. If we assume that the dominant balance is between ASR and SHF over the ocean and remove this energy balance, the resulting system of equations for the seasonal amplitude of energetics over land and ocean subdomains can be expressed by the matrix equation

$$\begin{pmatrix} -\frac{B_{ZHT}}{F_L} - F_L B_{MHT} - B_{CTEN} - [B_{OLR}] & \frac{B_{ZHT}}{LFRAC} - (1-F_L)B_{MHT} \\ \frac{B_{ZHT}}{F_L} - F_L B_{MHT} & -\frac{B_{ZHT}}{1-F_L} - (1-F_L)B_{MHT} - B_{CTEN} - [B_{OLR}] \end{pmatrix} \begin{pmatrix} |[T'_{A,L}]| \\ |[T'_{A,O}]| \end{pmatrix} = \begin{pmatrix} |ASR'| \\ 0 \end{pmatrix}, \quad (17)$$

where the first and second rows correspond to the energy balance in the atmosphere above the land and ocean sub-domains respectively. (In deriving equation (17), we have assumed that all of the ASR in the land domain is passed immediately to the atmosphere via the surface heat flux). The solution to (17) determines the seasonal amplitudes of atmospheric temperatures in the ocean and land subdomains and hence Δ (see equation (15)). The seasonal amplitude of the surface temperature in the land and ocean subdomains is then obtained using equations (14) and (16) respectively. Lastly, the seasonal energetics can be calculated by way of the temperatures and the B coefficients; all curves based on these equations are co-plotted in Fig. 6 and agree qualitatively with the EBM simulations[6].

The critical control parameter in the system is the land-ocean atmospheric temperature difference that governs the ZHT. In our pseudo equilibrium assumptions, the only external source of seasonal energy to the atmosphere is in the land subdomain (over the ocean subdomain, ASR goes into the ocean heat storage). This quantity of energy is fixed by the specified land fraction and ASR, and is a constraint to the land-ocean temperature contrast; the magnitude of the total zonal heat flux can not exceed the energy supplied at the source (ASR over land), otherwise the induced temperature changes would reverse the land sea temperature gradient driving the flux. In reality, less energy

[6] In the pseudo steady state balance, the seasonal cycle of ocean temperature (and thus the ocean SHF) is necessarily and unrealistically unchanging with land fraction (the blue dotted curves in Fig. 6a,c).

than the ASR integrated over the $F_L$ is available to transport zonally because MHT, OLR, and CTEN also scale with atmospheric temperature anomalies according their respective B coefficients which are smaller than $B_{ZHT}$, but not negligible. Thus, as the $F_L$ is increased, more energy is made available to the atmosphere to drive seasonal changes in ZHT to the ocean domain, as well as changes in MHT, OLR, and CTEN in both the ocean and land domain (Fig. 6)

There are limitations to the pseudo-equilibrium solution, mainly that we have assumed all of the ASR is absorbed in the ocean, thereby fixing the seasonal amplitude of the surface ocean temperature. Surprisingly, this assumption underestimates the ocean heat storage in the EBM; the presence of land ensures that, during the summer, the ocean surface layer absorbs more energy than is provided by the sun locally, especially as we increase the $F_L$. If we were to instantly turn off the EBM's heat transport in the middle of the summer, the atmosphere over the ocean would cool. This result is also true in the NH of the observed climate system. Essentially, a portion of the energy that is absorbed by the atmosphere over the land sub-domain during the summer finds it's way to storage below the ocean surface, just as a portion of the energy that is fluxed to the atmosphere from the ocean surface in the winter warms the continental atmosphere. Because the seasonal cycle is nearly symmetric about the equinoxes, these processes must be reflexive; a portion of solar insolation over the continent must find its way into the ocean mixed layer in order for the ocean to moderate the seasonal cycle over the continent.

We then can ask, what conditions must be met in order for the atmosphere to flux energy to the ocean? Energy is fluxed from the ocean surface to the atmosphere by way of latent and sensible heat fluxes and efficient (blackbody) radiation. In contrast, the atmosphere

fluxes energy to the underlying ocean as a less efficient radiator, and via sensible heat fluxes. Therefore the seasonal amplitude of the atmospheric temperature must exceed that of surface temperature in order for the net flux to be from the atmosphere to the ocean in the summer. We can calculate the $\kappa_O$ that must be deceeded in order to have a net flux into the ocean by setting the net SHF (denominator of (13)) to zero:

$$\kappa_{O,crit} < \frac{B_{SH} + \left[ B_{LW\downarrow} \right]}{B_{SH} + B_{LH} + B_{OLR,S}} = .37 . \tag{18}$$

The EBM achieves $\kappa_O$ values below this critical value for $F_L > .7$. In reality, the atmosphere can drive a heat flux into the ocean with a substantially higher kappa value (i.e., with a substantially lower land fraction), because the atmospheric temperatures are nearly in phase with ASR in the coupled system, where as the ocean temperatures lag the ASR by a couple of months.

**5. Summary and discussion**

We have formulated a very simple EBM model to understand the gross energetics of the seasonal climate system -- in particular, the relative importance of the processes that flux of energy between the tropics and the polar regions, and between the land and ocean regions. The advantage of this formulation is that the magnitude of the various energy fluxes can be understood in terms of their respective sensitivities (B coefficients). We have shown that the dominant processes that control the annual averaged and seasonal cycle of energy fluxes can be deduced from the model control parameters and pseudo steady state ideas.

In the annual mean, the polar region receives anomalously low (compared to the global average) absorbed solar radiation (ASR) that is balanced by meridional heat

transport (MHT), outgoing longwave radiation (OLR), and surface heat fluxes (SHF) associated with ocean heat transport in approximately a 6:3:2 ratio. The ratio between MHT and OLR is well replicated and easily understood in terms of the B coefficients in our EBM, which are derived from solving the basic state and parameterizations derived from observations and AGCM simulations.

On the seasonal time scale, the majority of the polar region ASR anomalies go into seasonal ocean storage, with smaller quantities of energy entering the atmosphere to drive seasonal changes in MHT, OLR, and the tendency in atmospheric energy storage (CTEN). The ratio of these component terms can be understood in terms of the relative B coefficients in our aqua-planet EBM framework. Furthermore, the fraction of energy supplied by ASR that goes into seasonal ocean storage versus that entering the atmosphere (to drive seasonal anomalies in OLR, MHT, and CTEN) is a strong function of mixed layer depth. This framework suggests that the energy flux processes that balance the seasonal cycle in ASR (and hence, the seasonal cycle of surface and atmospheric temperature) in the observed climate system is just as much a consequence of the ocean mixed layer depth as it is the Earth-Sun geometry. For example, as the ocean mixed layer depth decreases, the polar ASR anomalies become primarily balance by MHT, OLR and CTEN, with SHF playing a much smaller role; at ocean depths of less than 15 meters, the seasonal amplitudes of MHT, OLR, and the surface and atmospheric temperatures exceed the annual mean polar anomaly in magnitude, implying that the equator to pole temperature and OLR gradients reverse sign during the peak of summer, and the atmosphere transports heat from pole to equator. This is not an artifact of the simplicity of our EBM: the aqua-planet GCM simulations with less than 12 meters ocean

depth also exhibit this property. This result suggest that, as the equator to pole insolation gradient reverses in the summer, the only thing preventing the surface climate from following suite is the seasonal ocean heat storage. If this storage term were limited (i.e. in a snowball Earth), the Earth would exhibit an enhanced seasonal cycle in both temperature and meridional heat transport, the summer poles would momentarily exhibit the hottest climate on the planet, and heat would be exported from the poles to the tropics.

Land-ocean contrast in the zonal direction has a similar impact on the magnitude of the seasonal energetics as does the equator to pole insolation differences. This result is understandable in our model framework. Our model parameters suggests that nearly all of the ASR over the ocean goes into seasonal storage beneath the surface, where as nearly all the ASR over land enters the atmosphere immediately. Concurrently, the zonal atmospheric heat transport between the ocean and land is remarkable fast and efficient, transporting large quantities of energy from the seasonally warm sector to the seasonally cold sector. This transport acts to limit the seasonal cycle of temperature over land, and enhances the seasonal oceanic heat storage relative to the heat that would be stored considering local radiation alone. The land fraction plays a critical role in governing the magnitude of these processes. Essentially, the larger the fraction of the domain that is land, the larger effect it has on the ocean domain and vice versa. A large land domain leads primarily to more seasonal energy put into the atmosphere, driving seasonal changes in MHT, OLR, and CTEN above both land and ocean, and secondarily to more ZHT to the ocean that is taken up is seasonal heat storage. A large ocean domain limits

the net seasonal flux of energy to the atmosphere, thereby moderating the seasonal cycle of temperature, OLR, MHT, and CTEN, over both land and ocean.

Our results suggest that, on seasonal time scales, the local radiative (or other energy flux) perturbations exert a profound non-local effect on the coupled land-ocean climate system. For example, if a region of Arctic ocean that is usually ice covered in the winter becomes open ocean in a warmer world, the immediate effect is an additional heat flux out of the ocean in the winter. In fact, this change is a larger energetic anomaly than turning on the summer Sun over the region, because the magnitude of seasonal heat storage exceeds the local seasonal cycle of ASR (Section 4d) and therefore, is substantially larger than the radiative impact due to the albedo change of the melted ice. While the immediate impact is to warm the local atmosphere, our model framework tells us that, based on the B coefficients in the system, the majority of the energy (approximately 70% in the NH) will be fluxed zonally to the land domain. There, it will induce changes in MHT, OLR, CTEN, and the energy fluxed to the surface both radiatively and sensibly with the latter components composing approximately 40% of the initial heat that was fluxed zonally. At face value, only 30% of the initial energy perturbation finds its way to the land surface. However, whereas the initial perturbation will have a small impact on ocean temperatures, the equivalent amount of heat will have a large impact on the land surface, which has essentially no heat capacity and must come to radiative-convective equilibrium with the additional downwelling energy flux. Within our model framework, melting 10% of the polar winter ice would cause the average land surface temperature to increase by 0.6K. While our EBM is far too simple to be used to

make such predictions in the real climate system, it provides a framework for understanding seasonal energy balances such as these.

**Acknowledgements**

We thank Arnaud Czaja, whose work aided in our EBM conceptualization and some of the parameterizations implemented within the EBM. A similar seasonal EBM written by Cecilia Bitz also contributed to our model development. We also thank Dargan Frierson for implementing and running the slab ocean GCM runs and for his thoughtful feedback on the ideas presented in the manuscript. Gerard Roe's instruction helped to inspire our work on this subject area. This work was supported by NSF grant ATM-0502204 and the National Science Foundation's Graduate Fellowship Program.

## APPENDIX

### The energy balance model

Here we elaborate and provide justification for the parameterizations used in the EBM. We have diagnosed our parameterizations from linear best fits to the observations or, in some cases, simulations using an aquaplanet AGCM coupled to a slab ocean.

*a. Latent heat flux parameterization*

We diagnose a simple surface latent heat flux parameterization from the ensemble of five aquaplanet AGCM simulations described in section 2b by regressing the monthly mean latent heat flux against the monthly mean surface temperature for all data points and seasons collectively (Fig. 7a shows the 12 meter depth slab ocean regression). The regression coefficients from each of the runs are averaged to obtain the coefficient $B_{LH}$ in equation (1); the ensemble average $R^2$ value is 0.8. We chose to diagnose this relationship from AGCM simulations as opposed to observations because the AGCM diagnostics are more readily available and internally self consistent.

*b. Sensible Heat Flux Parameterization*

The surface to atmosphere sensible heat flux is also diagnosed from the aquaplanet AGCM runs by regressing the sensible heat flux against the difference between the surface temperature and the 900 hPa atmospheric temperature for all grid-points and months collectively (Fig. 7b). The linear best fits have an intercept that is significantly different from zero, as would be expected from the vertical lapse rate within the atmosphere. The ensemble average regression gives the coefficients $B_{SH}$ used in equation (2), (with an ensemble average $R^2$ value of 0.7), assuming that the lowest EBM

atmospheric layer can be substituted for the 900 hPa level. The constant $C_{SH}$ in equation (2) is then adjusted to account for the lowest EBM layer corresponding to a significantly higher level in the atmosphere than the 900 hPa level.

*c. Water vapor feedback factor*

Linearizing the radiation about the single column atmosphere mean state described in Section 2a, gives an OLR anomaly that can be expressed as a weighted average of the local $B_{OLR,N}$s with the weights representing the relative contribution of each layer to the radiation emitted to space:

$$OLR'\big|_{\varepsilon} = \sum_{N=1}^{4} B_{OLR,N} T_N' (\varepsilon_N \prod_{n=N+1}^{4} (1-\varepsilon_n)) \equiv \sum_{N=1}^{4} B_{OLR,N} T_N' W_N \ , \qquad \text{(A1)}$$

where $W_N$ is a normalized weighting coefficient. This expression states that, for a system with fixed layer emissivities, the inverse climate sensitivity for the entire column is the weighted average of the local $B_{OLR,N}$s, which vary from 5.3 W/m$^2$ at the surface (N=1) to 2.8 W/m$^2$ in the highest atmospheric layer in our basic state. All these values are significantly larger than the more commonly accepted values for inverse climate sensitivity (of order 2 Wm$^{-2}$K$^{-1}$, see Warren and Schneider 1979 for a discussion). Therefore, the weighted column average calculated from (A1) will not give a realistic inverse climate sensitivity (in our model, (A1) gives a value of 4 Wm$^{-2}$K$^{-1}$) unless the column mean emission temperature drops to approximately 200K.

The missing component is the water vapor feedback. The layer emissivities increase with increasing temperatures (due to the impact of water vapor on emissivity and temperature on water vapor via the Clausius Clayperon equation) leading to an upward shift of the emission level (i.e. the vertical weighting function) with increasing

atmospheric temperature. Therefore, a warmer column will emit from a higher level in the atmosphere where the basic state temperatures are colder (and the emitted longwave radiation is less energetic). This phenomenon partially offsets the increase in OLR from local heating of the column only (i.e. equation A1). We can take this into account while still maintaining the linearity in our model by decomposing the change in OLR into a component due directly to temperature change only and a component due to the change in emissivity (itself due to temperature change):

$$\frac{d(OLR')}{d([T'])} = \frac{\partial(OLR')}{\partial([T'])}\Big|_{\varepsilon} + \frac{\partial(OLR')}{\partial(\varepsilon)}\Big|_{[T']}\frac{\partial(\varepsilon)}{\partial([T'])} \approx C_{WV}\,\frac{\partial(OLR')}{\partial([T'])}\Big|_{\varepsilon}. \qquad \text{(A2)}$$

The fixed emissivity term was discussed above. The fixed temperature term is assessed to be -1.4 $Wm^{-2}K^{-1}$ in our 3-layer atmospheric mean state using Emanuel's (2002) formulation of emissivity with a fixed relative humidity of 70% and a $CO_2$ concentration of 350 ppm. $C_{WV}$ is the sum of the two terms divided by the fixed emissivity term and has a value of 0.65; it allows us to incorporate the water vapor feedback into the EBM while retaining linearity.

*d. Meridional heat transport*

We assume that the meridional heat flux divergence can be approximated by temperature diffusion:

$$MHT = D\nabla^2[T] \qquad , \qquad \text{(A3)}$$

where D is a diffusive parameter intended to capture the net effect of synoptic eddies and $\nabla^2$ is the spherical Laplacian. Taking the zonal mean of (A3) and Legendre expanding gives

$$A_{MHT,N} = D\frac{N(N+1)}{a^2}A_{T,N} \qquad \text{(A4)}$$

where $A_{MHT,N}$ and $A_{T,N}$ are the $N^{th}$ meridional wavenumber spectral coefficients in the zonal mean heat transport divergence and temperature respectively. We obtain the Legendre coefficients for the annual mean heat transport divergence and vertically averaged temperature from reanalysis data and determine *D* from (A4). If the heat transport were truly diffusive, each meridional wavenumber would determine the same value of *D*; in reality the calculated *D* values differ from one wavenumber to the next. We chose the value of *D* that is associated with meridional wave number 2 ($D = 0.95a^2$ $Wm^{-2}K^{-1}$ ) because meridional wavenumber 2 is the dominant scale associated with the equator to pole difference (this scale dominates the variance in both expansions).

We now relate this *D* value to the $B_{MHT}$ value used in equation (5). The *D* value must be multiplied by the spherical Laplacian eigenvalue which is $6a^{-2}$ at the equator to pole scale (wavenumber 2). Additionally, we recognize that the finite difference formulation of the diffusion equation used in (5) only approximates the spatial structure of the 2nd Legendre polynomial; in reality, the finite difference equation specifies a boxcar function with unit magnitude, changing signs at $30^0$. We determine how the EBM specification of the equator pole gradient relates to the Legendre coefficients in (A4) by projecting the boxcar function onto the 2nd Legendre polynomial; each unit of tropical-polar temperature difference in the EBM geometry corresponds to 0.63 units of the 2nd Legendre polynomial. Thus, the value D must be multiplied by these two geometric factors to get the value of $B_{MHT}$ specified in Section 2b.

*e. Zonal heat flux*

We diagnose the zonal heat flux parameterization from the reanalysis products. For each latitude between $20^0$N and $70^0$N (where land is prevalent), we first subtract the zonal averaged heat flux divergence (equivalently, the meridional heat transport divergence) from the heat flux divergence and then average the residual over the land domain; this quantity represents the heating over land due to zonal heat transport from the ocean domain. We then regress the (monthly) climatology of this quantity against the (monthly) climatological atmospheric temperature difference between the land and ocean domains, at each latitude separately (Fig. 7c). The resulting best fit slopes for each latitude (12 monthly points go into each regression) have fairly constant slopes with an average of -19 $Wm^{-2}K^{-1}$ corresponding to a zonal advection speed of 16 m/s if we assume that both the zonal temperature and heat flux divergence anomalies follow a zonal wavenumber 2 structure (corresponding to the presence of the American and Asian continents at these latitudes). This average slope is related to the ZHT parameterization given in Equation (6) by assuming that this data corresponds to a land fraction of approximately 50%. We postulate that the change in intercept with latitude seen in Fig. 7c results from more water vapor import from ocean to land in the low latitudes, where the ocean is warmer.

# References

Barkstrom, B. R., and J. B. Hall, 1982: Earth Radiation Budget Experiment (ERBE)—An overview. *J. Energy,* **6,** 141–146.

Berger, A.L., 1978: Long-term variations of caloric insolation resulting from Earth's orbital element, Quaternary Research,9, 139-167.

Budyko, M. I.,1969: The effect of solar radiation variations on the climate of the earth, *Tellus*, 21, 611-619.

Delworth, T. L., et al., 2006: GFDL's CM2 Global Coupled Climate Models. Part I: Formulation and simulation characteristics. *Journal of Climate*, 19(5), 643-674.

Emanuel, K., 2002: A simple model of multiple climate regimes, *J. Geophys. Res*., vol 107.

Enderton, D. and J. Marshall, 2009: Controls on the total dynamical heat transport of the atmosphere and oceans. *J. Atmos. Sci.*, 66, 1593-1611.

Fasullo, J. T., and K. E. Trenberth, 2008a: The annual cycle of the energy budget: Part I. Global mean and land-ocean exchanges, *J. Clim.,* 21, 2297–2312

Fasullo J., Trenberth K., 2008b. The annual cycle of the energy budget: Part II. Meridional structures and transports. *J Climate*, 21, 2313–2325.

Hartmann, D.L., 1994: Global Physical Climatology. Academic Press, 411 pages.

Lin, S-J., 2004: A "vertically Lagrangian" finite-volume dynamical core for global models. *Monthly Weather Review*, 132(10), 2293-2307.

North, G. R., 1975: Theory of energy-balance climate models, 1975. *J. Atmos. Sci.,* 32, 2033-2043.

North, G. R., and J. A. Coakley, 1978: Simple seasonacl limate models, *Meteorol. Gidrol.,* 5, 26-32.

Seager, R., D.S. Battisti, J. Yin, N. Naik, N. Gordon, A.C. Clement and M. Cane, 2002: Is the Gulf Stream responsible for Europe's mild winters? Q. J. R. Meteo. Soc., 128, 2563-86.

Sellers,W . D., 1969: A global climatic model based on the energy balance of the earth-atmosphere system. *J. Appl. Meteorol*., 8, 392-400.

Sellers, W.D., 1973: A new global climatic model. *J. Appl. Meteorol.* 12, 241-254.

Stone, P. H., 1978: Constraints on dynamical transports of energy on a spherical planet. *Dyn. Atmos. Oceans*, 2, 123–139.

Thompson S.L and S.H. Schneider, 1979: Seasonal zonal energy balance climate model with an interactive lower layer, J . Geophys. Res., 84, 2401-2414.

Trenberth, K. E., and J. M. Caron, 2001: Estimates of meridional atmosphere and ocean heat transports. *J. Climate*, 14, 3433–3443.

Trenberth, K.E. , J. M. Caron, and D. P. Stepaniak, 2001: The atmospheric energy budget and implications for surface fluxes and ocean heat transports. *Climate Dyn.,* **17,** 259–276.

Warren, S.G. and S.H. Schneider, 1979: Seasonal simulation as a test for uncertainties in the parameterizations of a Budyko-Sellers zonal climate model. *J.Atmos. Sci.,* 36, 1377-1391.

Wunsch, C., 2005: The total meridional heat flux and its oceanic and atmospheric partition. *J. Climate*, 18, 4374–4380.

Yang S, Olson WS, Wang J-J, Bell TL, Smith EA, Kummerow CD, 2006: Precipitation and latent heating distributions from satellite passive microwave radiometry. Part II: Evaluation of estimates using independent data. J. Appl. Meteor. Climatol. 45: 721–739.

## Figure Captions

Figure (1). (a) Zonal and annual averaged energy flux for ASR (red), OLR (green), SHF (blue), MHT (magenta), and CTEN (yellow). The global and annual average has been removed from each term. (c) Zonal averaged, seasonal anomaly energy flux for January (solid lines) and July (dotted lines). Energy flux terms separately over (b) land and (d) ocean areas for January (solid lines) and July (dotted lines). The zonal averaged heat flux divergence has been removed from all terms in (b) and (d). Also shown in (b) and (d) is the zonal heat flux (ZHT, black) over land and ocean, respectively. Data is for the Northern Hemisphere, and data sources are noted in section 2c.

Figure 2. (a) Seasonal amplitude of surface and vertically averaged atmospheric temperature in the polar regions as a function of mixed layer depth in the ensemble of aquaplanet EBM runs. The solid lines are from the EBM, asterisks are the aqua-planet GCM simulation. (b) As in (a) except for the seasonal energetics in the polar regions. The dashed lines are discussed in section 3b.

Figure 3. Global averaged seasonal energetics. All values are globally integrated seasonal anomalies from the global annual mean in PW. The dotted lines are the control six-box EBM simulation and the solid lines are the monthly mean observations.

Figure 4. Zonally averaged seasonal energetics over the 3 domains. All values are anomalies relative to the global annual average in PW. The dashed lines are the six-box

control EBM simulation and the solid lines are the monthly mean observations. The dashed vertical lines represent the solstices (blue and red) and equinoxes (green).

Figure 5. Seasonal energetics of the six-box EBM control run over the six subdomains. All values are seasonal anomalies from the local annual average in $Wm^{-2}$. The dashed lines are the control six-box EBM simulation and the solid lines are the monthly mean observations.

Figure 6.(a) Seasonal amplitude of surface and vertically averaged atmospheric temperatures over the land and ocean polar sub-domains as a function of $F_L$. (b) and (c) seasonal amplitude of energy fluxes over the land and ocean polar subdomains as a function of $F_L$. The solid lines are the results from the numerical integrations of the EBM. The dotted lines are the values based on pseudo-steady state ideas described in section 4d. The triangles on the left (right) side are the observations in the SH (NH).

Figure 7. (a) 12 meter depth Aquaplanet AGCM surface latent heat flux versus surface temperature for all gridpoints and seasons, plotted as a density function. The straight line is the linear best fit. (b) as in (a) except for the sensible heat flux (ordinate) and surface temperature minus 900 hPa temperature (abscissa). (c) The heat flux divergence due to land-ocean zonal heat transport (calculated from the reanalysis as described in the Appendix section e) versus the land-ocean vertically averaged temperature difference. Each set of the same colored dots represent the monthly mean values at a given latitude

and the corresponding colored line is the linear best fit to the data at that latitude. Only data between $20^0$N and $70^0$N are shown in these plots.

## Table Captions and Text

Table 1. Energy flux terms spatially integrated over the Northern Hemisphere polar domain. Note that each term has been integrated over the polar domain, and so is reported here in PW.

| | | Spatially Integrated Energy Divergence (PW) | | | | | |
|---|---|---|---|---|---|---|---|
| | | ASR | (-)OLR | SHF | MHT | ZHT | (-)CTEN |
| Annual and area averaged minus global annual average | Annual | -7.9 | 2.2 | 1.4 | 4.3 | | 0 |
| January minus annual average | January | -13.9 | 3 | 8.4 | 2.3 | | 0.2 |
| July minus annual average | July | 15.8 | -3.4 | -9.8 | -1.8 | | -0.8 |
| Average over OCEAN minus average over land (instantaneous) | January | 0.6 | -0.8 | 8.6 | 0 | -8.6 | 0.2 |
| | July | -0.2 | 0.4 | -5.2 | 0 | 5 | 0 |

Table 2. Summary of sensitivity coefficients used in the seasonal EBM.

| | $[B_{OLR}]$ | $B_{OLR,S}$ | $B_{SENS}$ | $B_{LH}$ | $B_{MHT}$ | $B_{ZHT}$ | $B_{LW\downarrow}$ | $B_{LW}$ |
|---|---|---|---|---|---|---|---|---|
| Coefficient value ($Wm^{-2}K^{-1}$) | 2.6 | 5.3 | 3 | 4 | 3.4 | 10 | 2.2 | 1.9 |

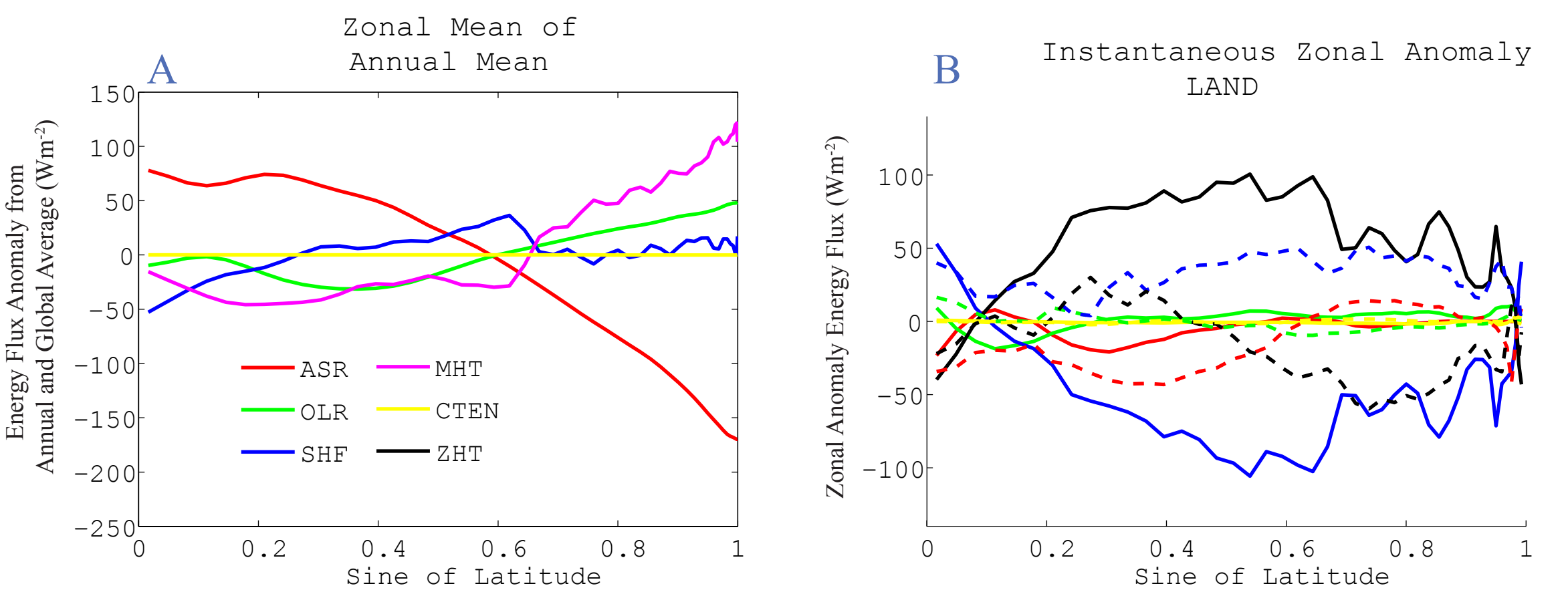


Figure (1). (a) Zonal and annual averaged energy flux for ASR (red), OLR (green), SHF (blue), MHT (magenta), and CTEN (yellow). The global and annual average has been removed from each term. (c) Zonal averaged, seasonal anomaly energy flux for January (solid lines) and July (dotted lines). Energy flux terms separately over (b) land and (d) ocean areas for January (solid lines) and July (dotted lines). The zonal averaged heat flux divergence has been removed from all terms in (b) and (d). Also shown in (b) and (d) is the zonal heat flux (ZHT, black) over land and ocean, respectively. Data is for the Northern Hemisphere, and data sources are noted in section 2c.

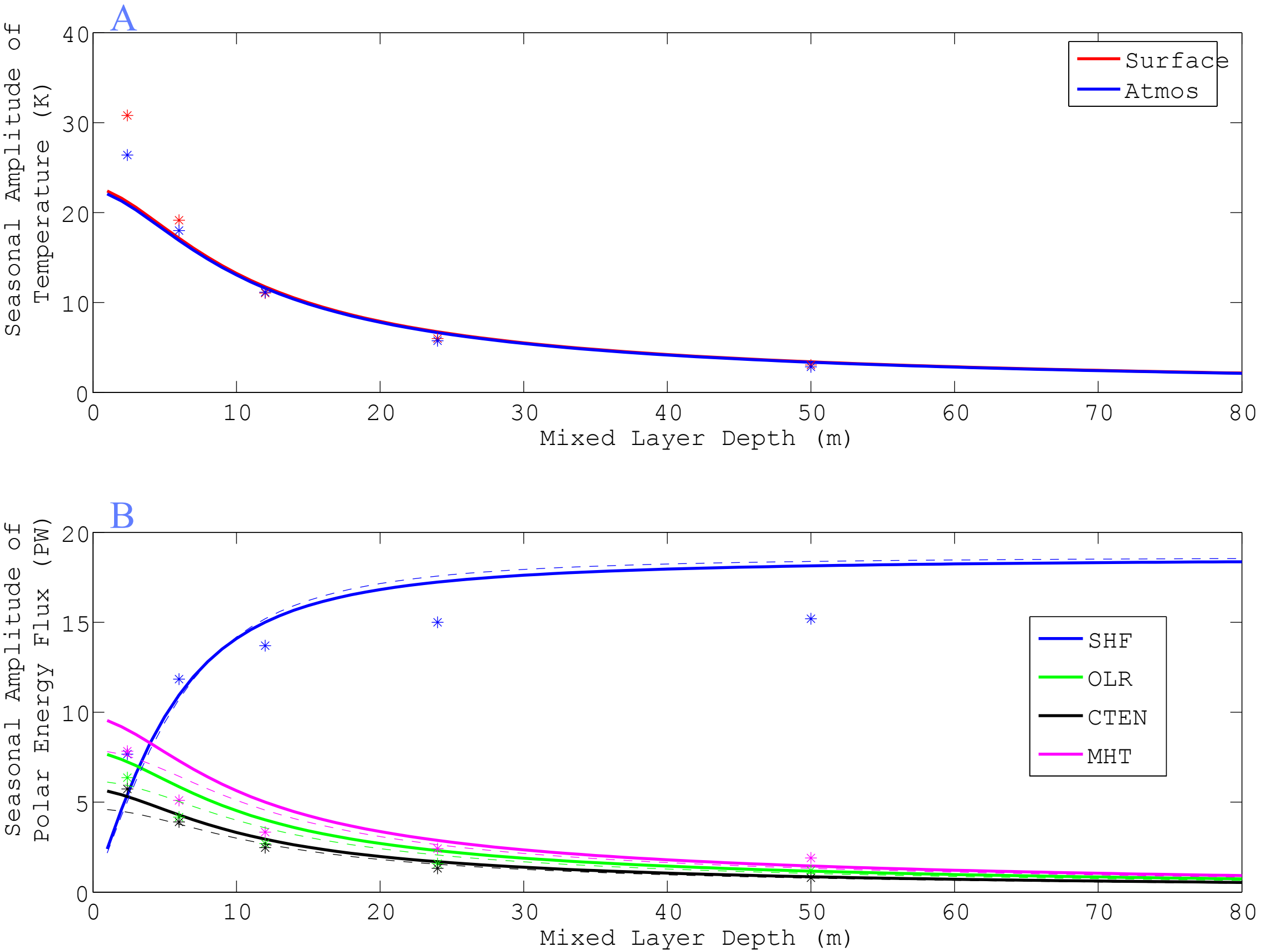


Figure 2. (a) Seasonal amplitude of surface and vertically averaged atmospheric temperature in the polar regions as a function of mixed layer depth in the ensemble of aquaplanet EBM runs. The solid lines are from the EBM, asterisks are the aquaplanet GCM simulation. (b) As in (a) except for the seasonal energetics in the polar regions. The dashed lines are discussed in section 3b.

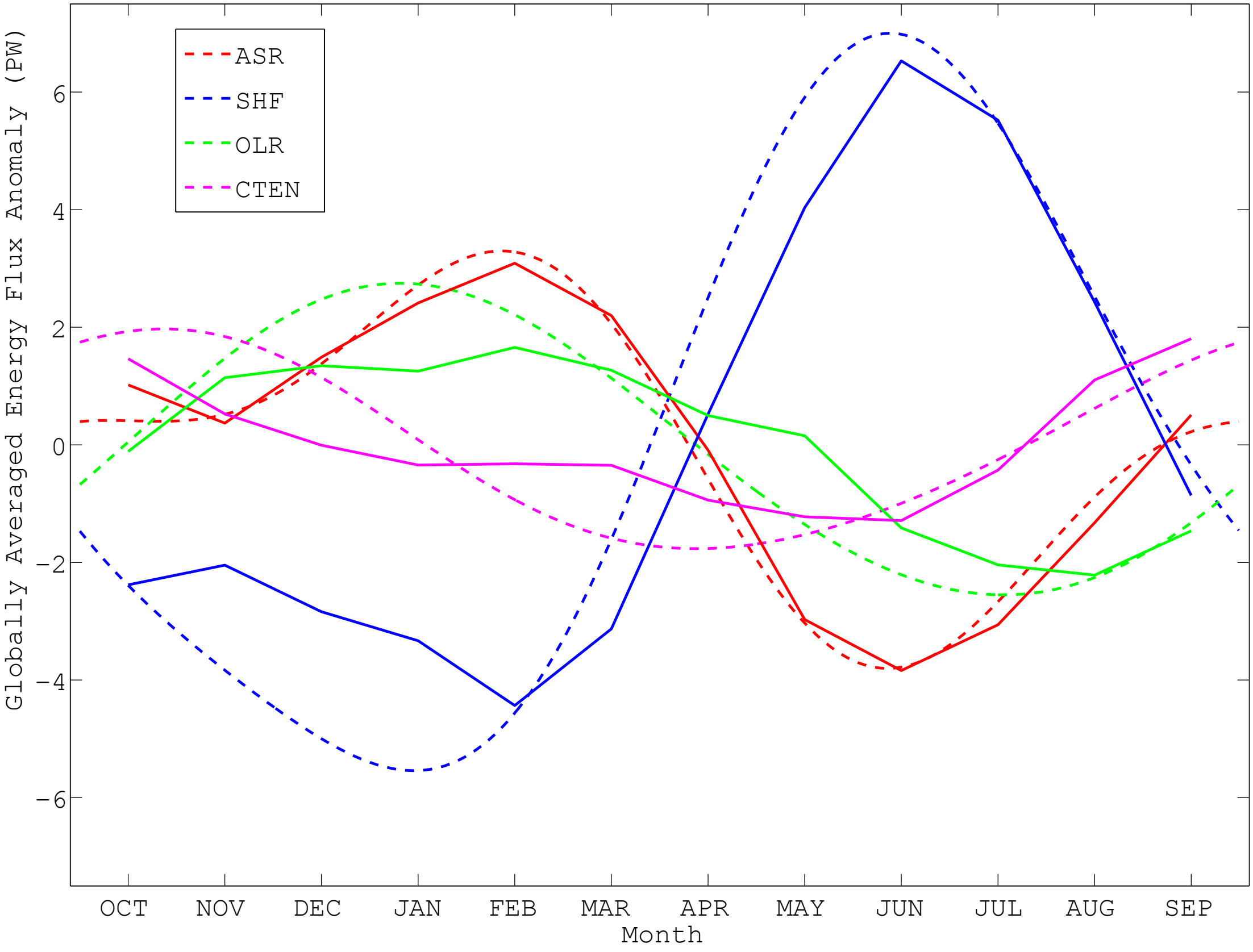


Figure 3. Global averaged seasonal energetics. All values are globally integrated seasonal anomalies from the global annual mean in PW. The dotted lines are the control six-box EBM simulation and the solid lines are the monthly mean observations.

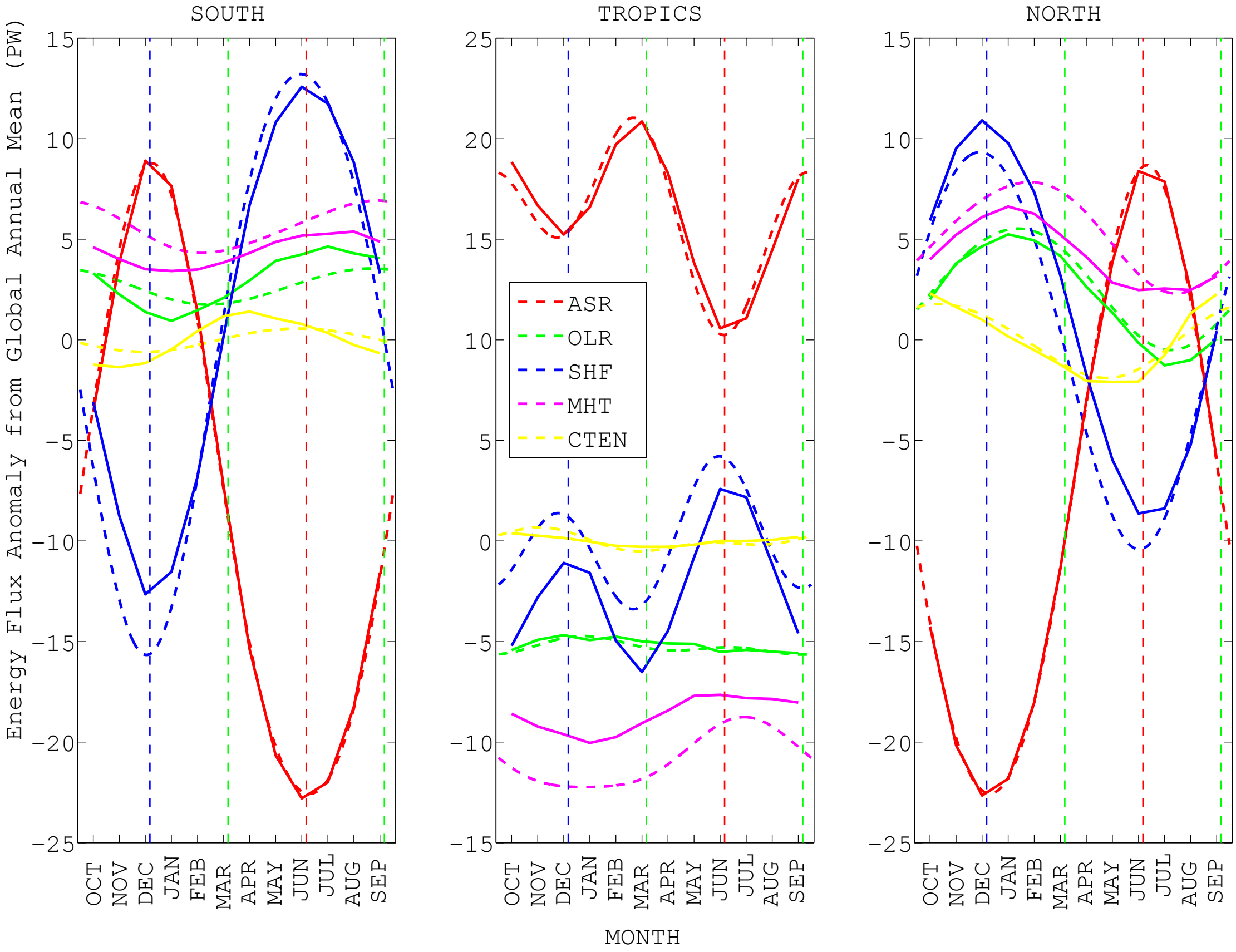


Figure 4. Zonally averaged seasonal energetics over the 3 domains. All values are anomalies relative to the global annual average in PW. The dashed lines are the six-box control EBM simulation and the solid lines are the monthly mean observations. The dashed vertical lines represent the solstices (blue and red) and equinoxes (green).

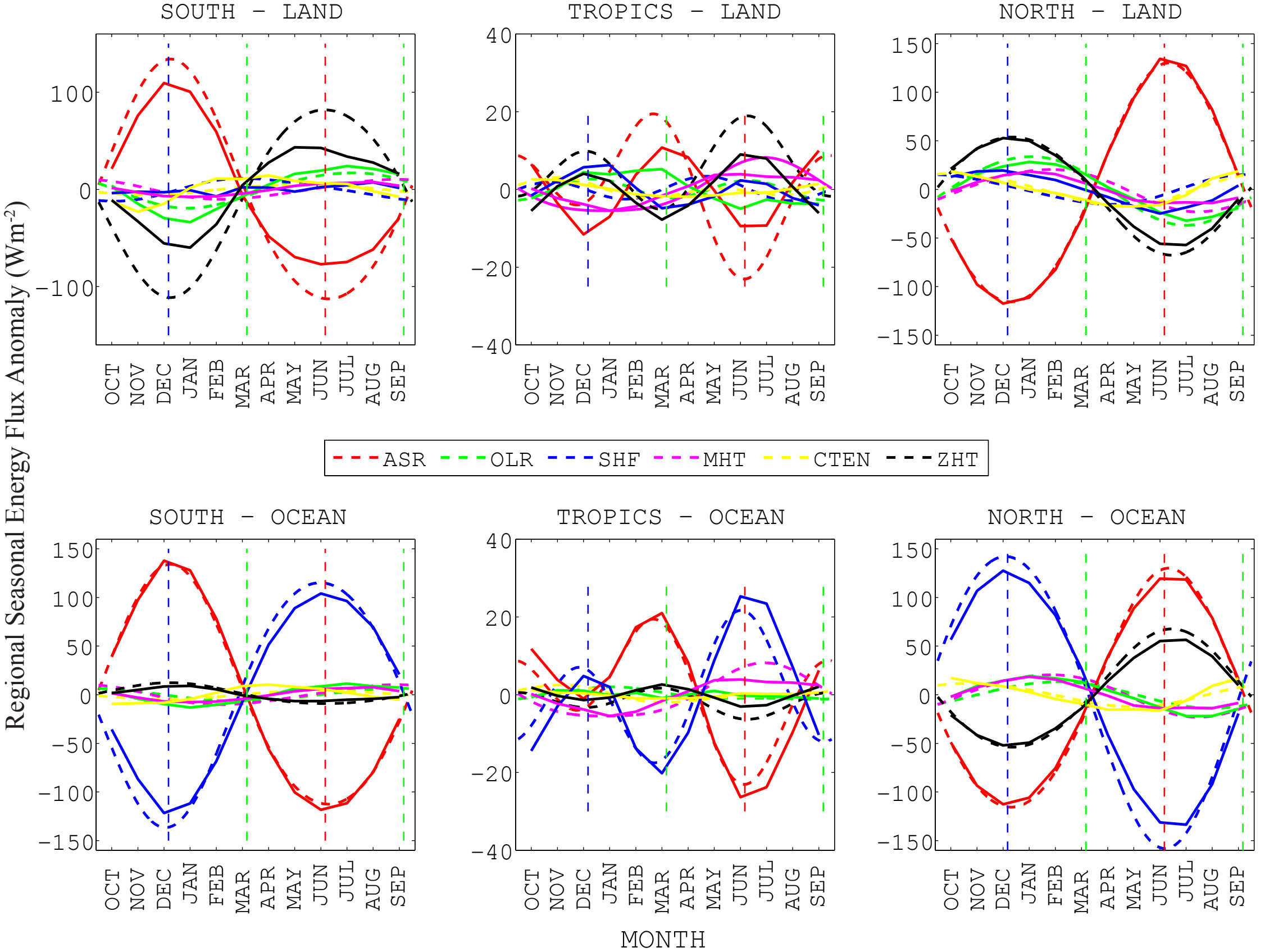


Figure 5. Seasonal energetics of the six-box EBM control run over the six subdomains. All values are seasonal anomalies from the local annual average in Wm-2. The dashed lines are the control six-box EBM simulation and the solid lines are the monthly mean observations.

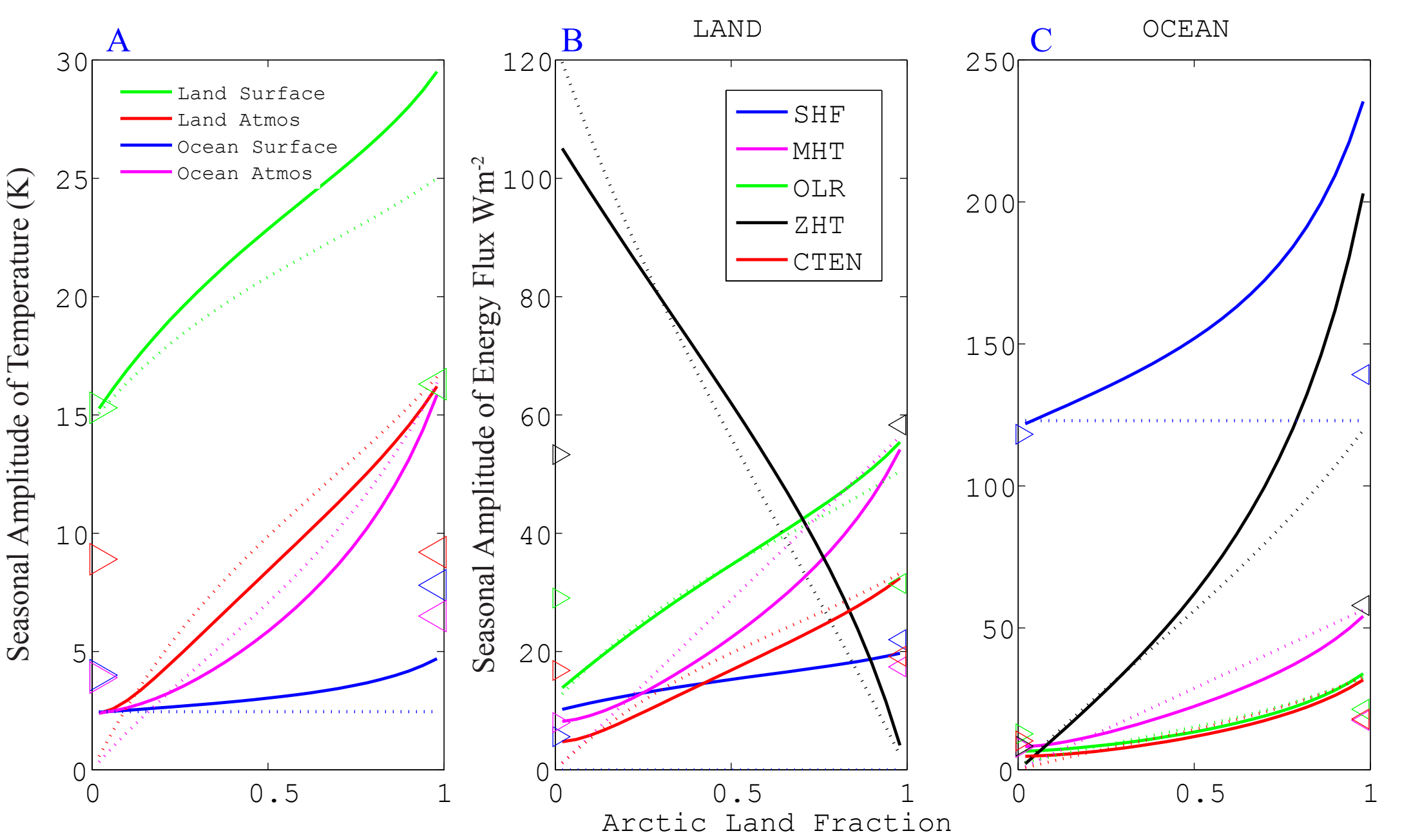


Figure 6.(a) Seasonal amplitude of surface and vertically averaged atmospheric temperatures over the land and ocean polar sub-domains as a function of FL. (b) and (c) seasonal amplitude of energy fluxes over the land and ocean polar subdomains as a function of FL. The solid lines are the results from the numerical integrations of the EBM. The dotted lines are the values based on pseudo-steady state ideas described in section 4d. The triangles on the left (right) side are the observations in the SH (NH).

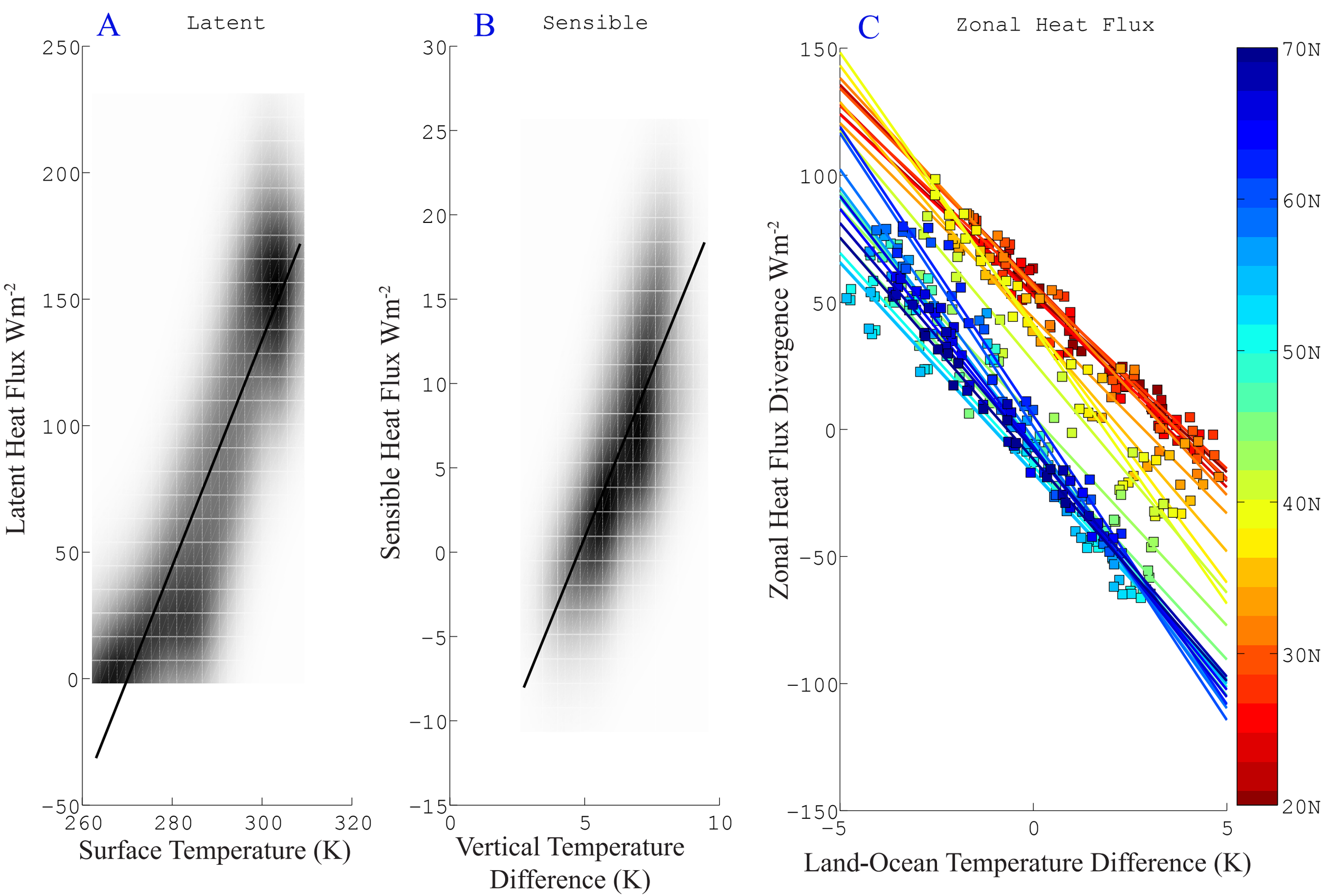


Figure 7. (a) 12 meter depth Aquaplanet AGCM surface latent heat flux versus surface temperature for all gridpoints and seasons, plotted as a density function. The straight line is the linear best fit. (b) as in (a) except for the sensible heat flux (ordinate) and surface temperature minus 900 hPa temperature (abscissa). (c) The heat flux divergence due to land-ocean zonal heat transport (calculated from the reanalysis as described in the Appendix section e) versus the land-ocean vertically averaged temperature difference. Each set of the same colored dots represent the monthly mean values at a given latitude and the corresponding colored line is the linear best fit to the data at that latitude. Only data between 200N and 700N are shown in these plots.